JPNT 4(4), 161-171 (2015)
http://dx.doi.org/10.11003/JPNT.2015.4.4.161

JPNT Journal of Positioning, Navigation, and Timing

Asynchronous Multilevel Search Strategy for Fast Acquisition of AltBOC Signals

Binhee Kim, Seung-Hyun Kong†
CCS Graduate School for Green Transportation, Korea Advanced Institute of Science and Technology, Daejeon 305-701, Korea

ABSTRACT

Alternative binary offset carrier (AltBOC) signals can be approximated by four synchronized direct sequence spread spectrum (DSSS) signals, each pair of which is a quadrature phase shift keyed (QPSK) signal at a different frequency. Therefore, depending on the strength of an incoming AltBOC signal, an acquisition technique can reduce the mean acquisition time (MAT) by searching the four DSSS signals asynchronously; the search for each of the four DSSS signals can start at one of the evenly separated hypotheses on the two-dimensional hypothesis space. And detection sensitivity can be improved by multiple levels when different numbers of search results for the same hypothesis are combined. In this paper, we propose a fast AltBOC acquisition technique that has an asynchronous search strategy and efficiently utilizes the output of the four search results to increase the sensitivity level when sensitivity improvement is needed. We provide a complete theoretical analysis and demonstrate with numerous Monte Carlo simulations that the MAT of the proposed technique is much smaller than conventional AltBOC acquisition techniques.

Keywords: AltBOC, acquisition, asynchronous search, search strategy

1. INTRODUCTION

The next-generation GNSS is being deployed (Parkinson et al. 1996, Kaplan & Hegarty 2005, Misra & Enge 2006), as planned. The U.S. government built a Global Positioning System (GPS) modernization plan that adds new civil and military signals to the legacy GPS (Kaplan & Hegarty 2005). The European Union is also deploying Galileo for civilian and public use (Kaplan & Hegarty 2005), Russia is planning to transmit a new civil signal from Global Navigation Satellite System, and the Chinese Compass system is expected to achieve a full operational capability by 2020 (Montenbruck et al. 2012).

Among the modulation schemes employed in the next-generation GNSS, alternating binary offset carrier (AltBOC) modulation has been adopted to the multiple new signals including Galileo E5 and Compass B2 signals. The AltBOC modulation belongs to the family of binary offset carrier (BOC) modulation. However, unlike the BOC modulation, AltBOC signals carry different signal components on each side of their split spectrum. For example, Galileo E5 has a double-sideband spectrum, where each sideband can be approximated by the spectrum of a quadrature phase shift keying (QPSK) modulated signal whose in-phase and quadrature-phase components are two different direct sequence spread spectrum (DSSS) signals. As a result, Galileo E5 signal offers unprecedented performance with a theoretical code tracking error less than 5 cm at signal strength of 35 dB-Hz (Sleewaegen et al. 2004), which is superior to other existing or planned GNSS signals. In addition, due to the multiple synchronized DSSS signals conveyed in an AltBOC signal, the detection sensitivity of the AltBOC signal can be higher than existing GNSS signals.

However, the enhanced performance of the AltBOC signals comes with a cost such as larger mean acquisition computation, longer mean acquisition time (MAT), or more receiver hardware complexity than a legacy GPS signal.

Received Sep 27, 2015 **Revised** Nov 23, 2015 **Accepted** Nov 23, 2015
†**Corresponding Author**
E-mail: skong@kaist.ac.kr
Tel: +82-42-350-1265 Fax: +82-42-350-1250

To reduce the cost for the fast AltBOC acquisition, a few techniques have been suggested to acquire the primary codes (the direct spreading sequence) of an AltBOC signal in the presence of the secondary code and unknown navigation data bits. For example, there are single side-band acquisition (SSB), double side-band acquisition (DSB), full-band independent code (FIC) acquisition, and Direct-AltBOC acquisition (Margaria et al. 2008, Shivaramaiah 2011) techniques. In the SSB technique (Margaria et al. 2008), a receiver uses a single bandpass filter (BPF) with 20.46 MHz bandwidth (BW) to acquire one or two primary codes in one of the two QPSK signals of the Galileo E5 signal, i.e., the technique may try to acquire one of the four primary codes in E5aQ, E5bQ, E5aI, and E5bI, or to acquire two primary codes in E5aI and E5aQ or in E5bI and E5bQ. In the DSB technique (Margaria et al. 2008), a receiver has two BPFs with 20.46 MHz BW to process two QPSK signals simultaneously and can non-coherently combine the search result of the two primary codes in {E5aQ, E5bQ} or the four primary codes in {E5aI, E5aQ, E5bI, and E5bQ}. However, in the FIC technique (Shivaramaiah 2011), a receiver has a BPF with 51.15 MHz BW and can non-coherently combine any set of the four primary code signals. Since a Galileo E5 signal is equivalent to an 8-PSK signal, in the Direct-AltBOC technique (Shivaramaiah 2011), a receiver is equipped with a BPF with 51.15MHz BW and correlates the incoming signal with a receiver replica of the 8-PSK signal generated with a look-up-table. In general, the DSB, FIC, and Direct-AltBOC techniques are preferred acquisition techniques to the SSB technique for higher detection sensitivity. However, due to the secondary code and unknown navigation data bits, the Direct-AltBOC technique has higher algorithmic and computational complexity than other techniques, and the FIC technique suffers from a larger noise power than the DSB technique for wider BPF bandwidth.

Despite of the multiplicity of the primary codes, all of the Galileo E5 signal acquisition techniques introduced in the literature employ a synchronized search strategy, where the code phase and Doppler frequency hypotheses of the primary codes being tested are always the same during the search process, and a single detection level strategy, where the number of auto-correlation function (ACF) outputs constructing a detection variable is fixed. In this paper, we propose a time-efficient asynchronous search strategy to reduce the MAT for AltBOC signal acquisition. The proposed strategy achieves about 4 times smaller MAT than the DSB and SSB techniques for a strong signal ($C/N_0 > 43$ dB) and has about similar MAT to the DSB and SSB techniques for moderate and weak signals ($C/N_0 < 36$ dB).

The rest of this paper is organized as follows. Section 2 introduces the Galileo E5 signal, and Section 3 introduces the conventional AltBOC signal acquisition techniques. The proposed asynchronous multilevel search strategy is introduced in Section 4. The statistical performance analysis of the proposed technique is provided in Section 5, and performance comparison to the conventional techniques using numerous Monte Carlo simulation results is provided in Section 6. The conclusion of the paper is in Section 7.

2. GALILEO E5 SIGNAL

Among a number of AltBOC signals in the next generation GNSS, we consider Galileo E5 signal as an example in this paper. The Galileo E5 signal consists of four sets of primary codes and secondary codes, and it can be modeled as the sum of two QPSK signals (i.e., E5a($=E_a^I \perp E_a^Q$) and E5b($=E_b^I \perp E_b^Q$)). In this regard, $A \perp B$ represents the phase difference between A and B, and $(\cdot)^I$ and $(\cdot)^Q$ represent the in-phase signal component and the quadrature-phase signal component, respectively. E5a($=E_a^I \perp E_a^Q$) and E5b($=E_b^I \perp E_b^Q$) signals are transmitted at a carrier frequency of 1176.45 MHz and 1207.14 MHz, respectively. For the Galileo E5 signal, the in-phase signal component is transmitted by spreading the navigation data bit signal as a primary code and a secondary code, and the quadrature-phase signal component is transmitted by spreading the pilot signal as another primary code and secondary code. The four signal components, E5a data channel (E_a^I), E5a pilot channel (E_a^Q), E5b data channel (E_b^I), and E5b pilot channel (E_b^Q), are spread by four synchronized primary codes of the same chip rate 10.23 MHz ($=fr$, where fr is the reference frequency) so that the main lobes of E5a and E5b spectra span $2fr$. The transmitted signal from Galileo E5 satellite is expressed (Galileo Project 2013)

$$\begin{aligned} s(t) = \frac{1}{2\sqrt{2}}\Big[& (E_a^I(t) + jE_a^Q(t))(sc_s(t) - jsc_s(t - \frac{T_{sc}}{4})) \\ & + (E_b^I(t) + jE_b^Q(t)(sc_s(t) + jsc_s(t - \frac{T_{sc}}{4})) \\ & + (\overline{E}_a^I(t) + j\overline{E}_a^Q(t)(sc_p(t) - jsc_p(t - \frac{T_{sc}}{4})) \\ & + (\overline{E}_b^I(t) + j\overline{E}_b^Q(t)(sc_p(t) + jsc_p(t - \frac{T_{sc}}{4}))\Big], \end{aligned} \tag{1}$$

where

$$\overline{E}_a^I(t) = E_a^Q(t)E_b^I(t)E_b^Q(t) \tag{2}$$
$$\overline{E}_a^Q(t) = E_a^I(t)E_b^I(t)E_b^Q(t) \tag{3}$$
$$\overline{E}_b^I(t) = E_a^I(t)E_a^Q(t)E_b^Q(t) \tag{4}$$
$$\overline{E}_b^Q(t) = E_a^I(t)E_a^Q(t)E_b^I(t) \tag{5}$$

http://dx.doi.org/10.11003/JPNT.2015.4.4.161

Table 1. AltBOC subcarrier coefficients.

k	a_k	b_k
1	$\sqrt{2}$+1	-$\sqrt{2}$+1
2	1	1
3	-1	-1
4	-$\sqrt{2}$-1	$\sqrt{2}$-1
5	-$\sqrt{2}$-1	$\sqrt{2}$-1
6	-1	-1
7	1	1
8	$\sqrt{2}$+1	-$\sqrt{2}$+1

are the product components

$$sc_s(t) = \sum_{k=1}^{8} a_k \cdot \mathrm{rect}_{T_{sc}}(t - kT_{sc}/8) \tag{6}$$

$$sc_p(t) = \sum_{k=1}^{8} b_k \cdot \mathrm{rect}_{T_{sc}}(t - kT_{sc}/8) \tag{7}$$

are the subcarrier functions of the signal and product components, respectively. T_{sc} denotes the subcarrier period, T_c(=1.5T_{SC}) denotes the chip width of the Galileo E5 signal, and the coefficients a_k and b_k are summarized in Table 1.

Since an AltBOC signal can be modeled as the sum of two QPSK signals separated in frequency by 3f_r, the incoming signal to a GNSS receiver can be expressed as

$$\begin{aligned} r(t) = {} & \alpha\left[E_a^I(t-\tau) + jE_a^Q(t-\tau)\right]e^{j(2\pi(f_{IF}+f_d^a-f_{sc})t+\phi_a)} \\ & + \alpha\left[E_b^I(t-\tau) + jE_b^Q(t-\tau)\right]e^{j(2\pi(f_{IF}+f_d^b+f_{sc})t+\phi_b)} \\ & + \beta r_p(t) + \omega(t), \end{aligned} \tag{8}$$

where $r_p(t)$ represents the sum of the product components as

$$\begin{aligned} r_p(t) = {} & \alpha\left[\overline{E}_a^I(t-\tau) + j\overline{E}_a^Q(t-\tau)\right]e^{j(2\pi(f_{IF}+f_d^a-f_{sp})t+\phi_c)} \\ & + \alpha\left[\overline{E}_b^I(t-\tau) + j\overline{E}_b^Q(t-\tau)\right]e^{j(2\pi(f_{IF}+f_d^b+f_{sp})t+\phi_d)} \end{aligned} \tag{9}$$

and τ, f_{IF}, f_d^a, f_d^b, f_{sc}, and f_{sp} are the code phase, IF frequency, Doppler frequency of the E5a channel, Doppler frequency of E5b channel, subcarrier frequency 1.5f_r of the signal components, subcarrier frequency of the product components, respectively, ϕ_a, ϕ_b, ϕ_c, and ϕ_d are unknown phase offsets, α and β represent magnitudes, and $w(t)$ is a complex additive white Gaussian noise with two-sided power spectral density $\frac{N_0}{2}$. The received power ratio between the signal components α^2 and the product components β^2 is about 6 (Lestarquit et al. 2008). Note that the maximum difference f_d^a between f_d^b and is 65Hz due to the difference of the carrier frequencies of E5a and E5b signals (Wallner et al. 2005). When T = 1 ms is the integration interval and 1/(2T) = 500 Hz is the frequency search step size (assumed in this paper), the 65 Hz difference is negligible so that we can further assume $f_d^a \approx f_d^b \approx f_d$ without loss of generality.

3. CONVENTIONAL ALTBOC SIGNAL ACQUSISTION

The front end of a GNSS receiver uses a number of analogue filters whose precise characteristics are difficult to model with theoretical expressions. However, for an algebraic simplicity in this paper, we assume that a filter $H_v(f)$ in the front end is an ideal linear bandlimited filter such that the amplitude response and the derivative of the phase response with respect to the frequency f are constant as

$$|H_v(f)| = A_v \tag{10}$$

$$-\frac{1}{2\pi}\frac{d\psi_v(f)}{df} = \tau_v \tag{11}$$

respectively, for all frequency f within the passband of bandwidth B_v, where $\psi_v(f) = \angle H_v(f)$ and $v \in \{1,2,3\}$ is the filter index so that the filter transfer function can be expressed as

$$H_v(f) = A_v e^{j(-2\pi f\tau_v+\theta_v)} = (A_v e^{j\theta_v})e^{-j2\pi f\tau_v}, \tag{12}$$

where θ_v is a phase offset. In addition, $\tau_v << Tc$ and $A_v = 1/\sqrt{B_v}$ are assumed for an ideal filter, and, in the following, $h_v(t)$ denotes the time-domain expression of $H_v(f)$.

In the following, among a few conventional AltBOC acquisition techniques introduced in the literature, Direct-AltBOC, SSB, and DSB techniques, shown in Fig. 1, respectively, are briefly introduced for a comparison with the proposed technique in Section 6. The detection variable of the Direct-AltBOC technique is found in (Shivaramaiah 2011) as

$$\begin{aligned} y_1 = \sum_{n=0}^{N_T-1} r_x[n] \Bigg[& \left(E_a^I[n-\hat{n}_\tau] + j\cdot E_a^Q[n-\hat{n}_\tau]\right)\times\left(sc_s[n-\hat{n}_\tau] - j\cdot sc_s\left[n-\hat{n}_\tau-\frac{n_{sc}}{4}\right]\right) \\ & + \left(E_b^I[n-\hat{n}_\tau] + j\cdot E_b^Q[n-\hat{n}_\tau]\right)\times\left(sc_s[n-\hat{n}_\tau] + j\cdot sc_s\left[n-\hat{n}_\tau-\frac{n_{sc}}{4}\right]\right) \\ & + \left(\overline{E}_a^I[n-\hat{n}_\tau] + j\cdot \overline{E}_a^Q[n-\hat{n}_\tau]\right)\times\left(sc_p[n-\hat{n}_\tau] - j\cdot sc_p\left[n-\hat{n}_\tau-\frac{n_{sc}}{4}\right]\right) \\ & + \left(\overline{E}_b^I[n-\hat{n}_\tau] + j\cdot \overline{E}_b^Q[n-\hat{n}_\tau]\right)\times\left(sc_p[n-\hat{n}_\tau] + j\cdot sc_p\left[n-\hat{n}_\tau-\frac{n_{sc}}{4}\right]\right)\Bigg] \end{aligned} \tag{13}$$

where

$$r_x(t) = (h_1(t) * r(t))e^{-j2\pi(f_{IF}+f_d)t}, \tag{14}$$

$N_T = f_s T$, f_s and T denote the sampling frequency and the integration interval, respectively, $\hat{n}_\tau$ and n_{sc} denote the discrete-time representation of the estimated code delay

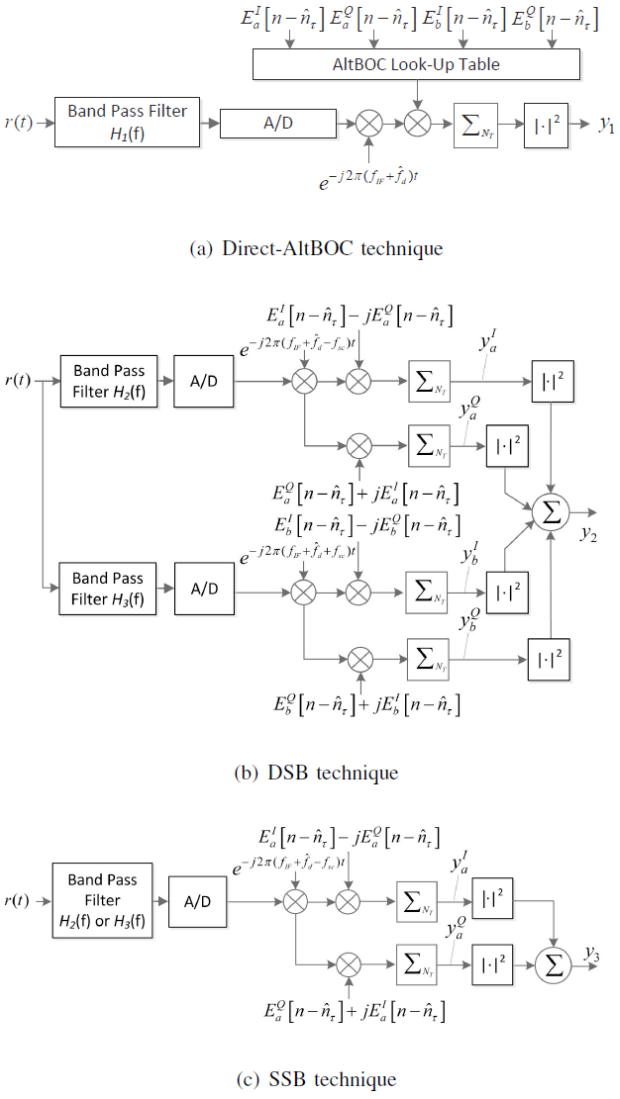

(a) Direct-AltBOC technique

(b) DSB technique

(c) SSB technique

Fig. 1. Conventional AltBOC acquisition.

$\hat{\tau}$ and T_{sc}, respectively, and $\hat{f}_d$ is the estimated Doppler frequency of the incoming signal $r(t)$. As shown in Fig. 1a, the filter $H_1(f)$ has the bandwidth $5f_c$ centering on the carrier frequency of Galileo E5. On the other hand, in Fig. 1c, E5a and E5b signals are filtered by different filters having the same bandwidth. In the DSB technique, four DSSS signals are despread and integrated to yield (Shivaramaiah 2011)

$$y_a^I = \sum_{n=0}^{N_T-1} r_a[n](E_a^I[n-n_\tau] - jE_a^Q[n-n_\tau]) \tag{15}$$

$$y_a^Q = \sum_{n=0}^{N_T-1} r_a[n](E_a^Q[n-n_\tau] + jE_a^I[n-n_\tau]) \tag{16}$$

$$y_b^I = \sum_{n=0}^{N_T-1} r_b[n](E_b^I[n-n_\tau] - jE_b^Q[n-n_\tau]) \tag{17}$$

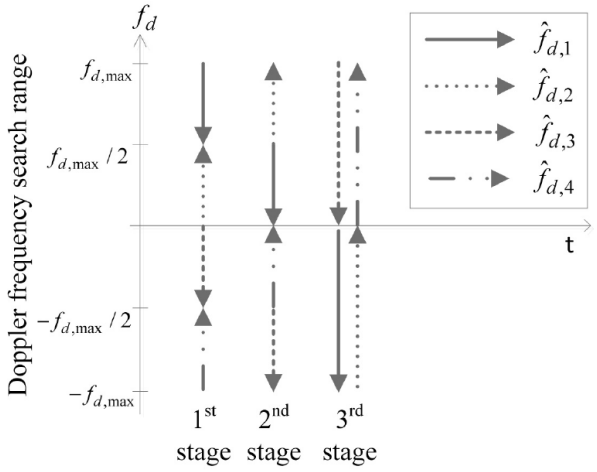

Fig. 2. Proposed asynchronous multilevel search strategy.

$$y_b^I = \sum_{n=0}^{N_T-1} r_b[n](E_b^Q[n-n_\tau] - jE_b^I[n-n_\tau]), \tag{18}$$

where

$$r_a(t) = (h_2(t) * r(t))e^{-j2\pi(f_{IF}+f_d-f_{sc})t} \tag{19}$$

$$r_b(t) = (h_2(t) * r(t))e^{-j2\pi(f_{IF}+f_d+f_{sc})t}, \tag{20}$$

and then the four outputs are non-coherently combined to build a detection variable (Shivaramaiah 2011)

$$y_2 = \left|y_a^I\right|^2 + \left|y_a^Q\right|^2 + \left|y_b^I\right|^2 + \left|y_b^Q\right|^2 \tag{21}$$

that has a non-central or central χ^2 distribution with 4 degrees of freedom (DOF) depending on the accuracy of $\hat{\tau}$ and $\hat{f}_d$. Using Eqs. (15-18), the detection variable of the SSB technique can be expressed as (Shivaramaiah 2011)

$$\begin{aligned} y_3 &= \left|y_a^I\right|^2 + \left|y_a^Q\right|^2 \\ &= \left|y_b^I\right|^2 + \left|y_b^Q\right|^2 \end{aligned} \tag{22}$$

that has a non-central or central χ^2 distribution with DOF 2 depending on the accuracy $\hat{\tau}$ of and $\hat{f}_d$.

4. PROPOSED TECHNIQUE FOR A FAST ALTBOC ACQUSITION

In this section, we describe the details of the proposed AltBOC acquisition technique, shown in Figs. 2 and 3. Fig. 2 illustrates the asynchronous search strategy employed in the three stages of the proposed technique, where the overall Doppler frequency search range is divided into four equal size small range segments that are searched in

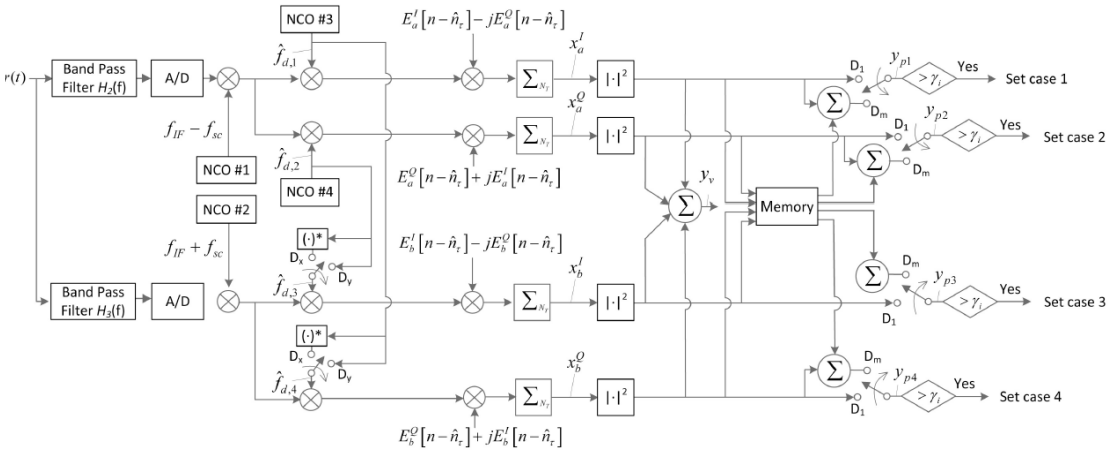

Fig. 3. Schematic diagram for proposed technique

parallel. The size of a range segment and the direction of the Doppler frequency search step increase are represented by arrows along the Doppler frequency axis for three stages. At the 1st stage, the four DSSS signals of Galileo E5 are searched in parallel and asynchronously such that the Doppler frequency hypotheses for the four DSSS signals are within the four respective range segments. The four arrows illustrate the initial Doppler frequencies and the final Doppler frequencies for each of the four DSSS signal searches in three stages. In the 2nd stage, the four arrows for the four DSSS signals continues in the same direction to search the four DSSS signals in the next Doppler frequency range segments. In the 3rd stage, the four arrows for the four DSSS signals are doubled in length so that the search of the four DSSS signals can be completed for all Doppler frequencies. Note that during the 1st (2nd) stage the AltBOC signal is completely searched over the entire two-dimensional hypothesis plane by testing only one (two) of the four DSSS signals at each hypothesis.

And during the first (second) half of the 3rd stage, the proposed technique can search the AltBOC signal using the three (four) of the four DSSS signals for all hypotheses. For algebraic simplicity in this paper, we assume that the search result of the first half of the 3rd stage is only stored in the memory block shown in Fig. 3 and the comparison of the detection variable to the detection threshold is only performed in the second half.

Fig. 3 shows the schematic diagram of the proposed technique. The two QPSK signals in $r(t)$ are filtered, sampled with sampling frequency $f_s = 1/T_s$, and carrier removed. The switches associated with numerically controlled oscillators (NCO) are on D_x nodes while the signal search is in process but on D_y in the verification mode. Notice that the conjugate of the NCO output is to generate a carrier with a negative frequency of the given input frequency, which is shown in Fig. 4. There

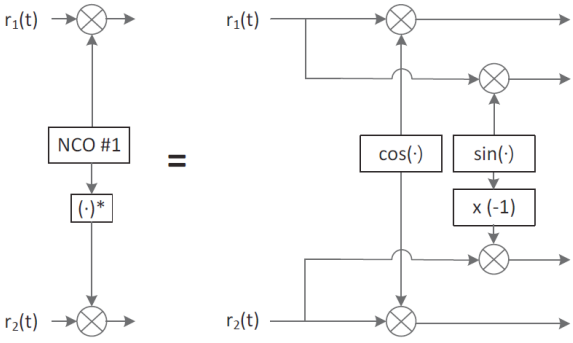

Fig. 4. Implementation of NCO.

are four arms for the four DSSS signals in the diagram, and each arm represents a path of a complex signal. The complex correlations are integrated for N_T samples and yield

$$x_a^I(\hat{f}_d) = \sum_{n=0}^{N_T-1} (h_2(t) * r(t)) e^{-j2\pi(f_{IF}+f_{d,1}-f_{sc})t} \times (E_a^I[n-n_\tau] - jE_a^Q[n-n_\tau]) \quad (23)$$

$$x_a^Q(\hat{f}_d) = \sum_{n=0}^{N_T-1} (h_2(t) * r(t)) e^{-j2\pi(f_{IF}+f_{d,2}-f_{sc})t} \times (E_a^Q[n-n_\tau] + jE_a^I[n-n_\tau]) \quad (24)$$

$$x_b^I(\hat{f}_d) = \sum_{n=0}^{N_T-1} (h_3(t) * r(t)) e^{-j2\pi(f_{IF}+f_{d,3}+f_{sc})t} \times (E_b^I[n-n_\tau] - jE_b^Q[n-n_\tau]) \quad (25)$$

$$x_b^Q(\hat{f}_d) = \sum_{n=0}^{N_T-1} (h_3(t) * r(t)) e^{-j2\pi(f_{IF}+f_{d,4}-f_{sc})t} \times (E_b^Q[n-n_\tau] + jE_b^I[n-n_\tau]) \quad (26)$$

where $\hat{n}$ is the code phase hypothesis for all four DSSS signals, and $\hat{f}_{d,m}$(m=1,2,3,4) is the Doppler frequency hypothesis for the -th DSSS signal. Since $\hat{f}_{d,m} \neq \hat{f}_{d,k}$ for any m≠k(m, k∈{1,2,3,4}), the 1st stage has four detection variables, $y_{p,m}$(m=1,2,3,4), that are compared to a common threshold γ_1 of the 1st stage.

$$y_{p1}|_{i=1} = \left| x_a^I(\hat{f}_{d,1}) \right|^2 \quad (27)$$

$$y_{p2}|_{i=1} = \left| x_a^Q(\hat{f}_{d,2}) \right|^2 \quad (28)$$

$$y_{p3}\,|_{i=1} = \left|x_b^I\left(\hat{f}_{d,3}\right)\right|^2 \tag{29}$$

$$y_{p4}\,|_{i=1} = \left|x_b^Q\left(\hat{f}_{d,4}\right)\right|^2 \tag{30}$$

where $\hat{f}_{d,4} = -\hat{f}_{d,1}$ and $\hat{f}_{d,3} = -\hat{f}_{d,2}$. In addition, $y_{p,m}$(m=1,2,3,4) for all $\hat{n}$ and $\hat{y}_{d,m}$ is stored in the memory block to use in later stages. When γ_1 is sufficiently high, and the code phase hypothesis and m-th Doppler frequency hypothesis $\hat{f}_{d,m}$ are correct, there can be only one decision block declaring a signal detection. When the signal detection at the m-th decision block is declared, we set $\hat{f}_{d,1}$ and $\hat{f}_{d,2}$ to $\hat{f}_{d,m}$ ('case m' in Fig. 3), set the switches associated with the NCOs over to nodes, and perform the verification using a combined detection variable y_p.

$$y_v = \left|x_a^I\left(\hat{f}_d\right)\right|^2 + \left|x_a^Q\left(\hat{f}_d\right)\right|^2 + \left|x_b^I\left(\hat{f}_d\right)\right|^2 + \left|x_b^Q\left(\hat{f}_d\right)\right| \tag{31}$$

If the signal is not detected in the 1st stage, the proposed technique performs the 2nd stage search, where the switches before the decision blocks are on D_m nodes, and every new ACF output is combined with the stored search result for the same code phase and Doppler frequency hypotheses in the 1st stage. Therefore, there are four detection variables in the 2nd stage as

$$y_{p1}\,|_{i=1} = \left|x_a^I\left(\hat{f}_{d,1}\right)\right|^2 + \left|x_a^Q\left(\hat{f}_{d,1}\right)\right|^2 \tag{32}$$

$$y_{p2}\,|_{i=1} = \left|x_a^Q\left(\hat{f}_{d,2}\right)\right|^2 + \left|x_a^I\left(\hat{f}_{d,2}\right)\right|^2 \tag{33}$$

$$y_{p4}\,|_{i=1} = \left|x_b^Q\left(\hat{f}_{d,4}\right)\right|^2 + \left|x_b^I\left(\hat{f}_{d,4}\right)\right|^2 \tag{34}$$

$$y_{p4}\,|_{i=1} = \left|x_b^Q\left(\hat{f}_{d,4}\right)\right|^2 + \left|x_b^I\left(\hat{f}_{d,4}\right)\right|^2 \tag{35}$$

where the second terms of the equations in Eqs. (32-35) are from the memory block that stores the search results (Eqs. (27-30)) of the 1st stage. The detection variables of the 2nd stage are also stored in the memory block for a possible use in the 3rd stage. When the signal is not detected in the 2nd stage, the proposed technique performs the 3rd stage search, where the switches before the decision block are on D_m nodes, and every new search result is combined with the stored search result for the same code phase and Doppler frequency hypotheses in the previous stages. The four 3rd stage detection variables are

$$y_{p1}\,|_{i=1} = \left|x_a^I\left(\hat{f}_{d,1}\right)\right|^2 + \left|x_a^Q\left(\hat{f}_{d,1}\right)\right|^2 + \left|x_b^Q\left(\hat{f}_{d,1}\right)\right|^2 + \left|x_b^I\left(\hat{f}_{d,1}\right)\right|^2 \tag{36}$$

$$y_{p2}\,|_{i=1} = \left|x_a^Q\left(\hat{f}_{d,2}\right)\right|^2 + \left|x_a^I\left(\hat{f}_{d,2}\right)\right|^2 + \left|x_b^I\left(\hat{f}_{d,2}\right)\right|^2 + \left|x_b^Q\left(\hat{f}_{d,2}\right)\right|^2 \tag{37}$$

$$y_{p3}\,|_{i=1} = \left|x_b^I\left(\hat{f}_{d,3}\right)\right|^2 + \left|x_b^Q\left(\hat{f}_{d,3}\right)\right|^2 + \left|x_a^Q\left(\hat{f}_{d,3}\right)\right|^2 + \left|x_a^I\left(\hat{f}_{d,3}\right)\right|^2 \tag{38}$$

$$y_{p4}\,|_{i=1} = \left|x_b^Q\left(\hat{f}_{d,4}\right)\right|^2 + \left|x_b^I\left(\hat{f}_{d,4}\right)\right|^2 + \left|x_a^I\left(\hat{f}_{d,4}\right)\right|^2 + \left|x_a^Q\left(\hat{f}_{d,4}\right)\right|^2 \tag{39}$$

where the second, third and fourth terms of the equations in Eqs. (36-39) correspond to the search results obtained during the first half of the 3rd stage that takes $N_A T$ seconds, the 1st stage (Eqs. (27-30)), and the 2nd stage (Eqs. (27-30)), respectively, that are stored in the memory block. Notice that by the end of the 3rd stage every code phase and Doppler frequency hypotheses is tested using a detection variable made from the search result(s) of one, two, and four of the four DSSS signals in the 1st, 2nd, and 3rd stages, respectively, which enables the multilevel detection sensitivity of the proposed technique.

5. PERFORMANCE ANALYSIS

In this section, we derive algebraic expressions for the performance analysis of the SSB, DSB, AltBOC, and proposed techniques.

5.1 Conventional DSB and SSB Techniques

The magnitude of an ACF output for the correct code phase and Doppler frequency hypotheses (cell) in the DSB and SSB techniques can be expressed using y_2 (Eqs. (32-35)) and y_3 (Eqs. (36-39)) as

$$S = \begin{cases} \sqrt{y_2}, & \text{for DSB} \\ \sqrt{y_3}, & \text{for SSB,} \end{cases} \tag{40}$$

respectively, and the noise variance can be found as

$$S = \begin{cases} 4 f_s T N_0, & \text{for DSB} \\ 2 f_s T N_0, & \text{for SSB.} \end{cases} \tag{41}$$

In the case of the DSB technique, the distribution of y_2 is a noncentral χ^2 distribution with DOF 4 for the H_1 cell as

$$P_0(y_2) = \frac{1}{V}\exp\left(\frac{-(y_2+S^2)}{V}\right)\sqrt{\frac{y_2}{S^2}}I_0\left(\frac{2S\sqrt{y_2}}{V}\right), \tag{42}$$

where $I_1(\cdot)$ is the first-order modified Bessel function of the first kind. And the distribution of y_2 for an incorrect hypothesis (H_0 cell) has a central χ^2 distribution with DOF 4 as

$$P_0(y_2) = \frac{y_2}{V^2}\exp\left(\frac{-y_2}{V}\right). \tag{43}$$

In the case of the SSB technique, the distribution of y_3 for the H_1 cell is a noncentral χ^2 distribution with DOF 2 as

$$P_1(y_3) = \frac{1}{V}\exp\left(\frac{-(y_3+S^2)}{V}\right)I_0\left(\frac{2S\sqrt{y_3}}{V}\right), \tag{44}$$

where $I_0(\cdot)$ is the zeroth-order modified Bessel function of

the first kind. On the other hand, for an cell has a central distribution with DOF 2

$$P_0(y_3)=\frac{1}{V}\exp\left(\frac{-y_3}{V}\right). \quad (45)$$

Using P_1 (Eqs. (42) and (45)) and P0 (Eqs. (43) and (45)), the false alarm, detection, and misdetection probabilities are (Abu-Rgheff 2007)

$$P_F(\gamma_0)=\left[1+\frac{\gamma_0}{V}\right]^{\frac{e}{2}}\exp(-\frac{\gamma_0}{V}) \quad (46)$$

$$P_D(\gamma_0)=Q_c\left(S\sqrt{\frac{2}{V}},\sqrt{\frac{2\gamma_0}{V}}\right) \quad (47)$$

$$P_M(\gamma_0)=1-P_D(\gamma_0), \quad (48)$$

respectively, where $g(a,b)$ is the lower incomplete Gamma function, $c=0$ for SSB, $c=2$ for DSB, and $Q_M(a,b)$ is the Marcum's Q-function (Marcum 1950) of order M as

$$Q_M(a,b)=\int_b^\infty u\left(\frac{u}{a}\right)^{M-1}\exp\left[\frac{-\left(u^2+a^2\right)}{2}\right]I_{M-1}(au)du. \quad (49)$$

5.2 First and second Stages of the Proposed Technique

In the following subsections, $y_{p,i}$ denotes the detection variable at the i-th stage (i=1,2,3) of the proposed technique. The ACF peak of the -th stage for the H_1 cell is

$$S_i=\sqrt{y_{p,i}}, \quad (50)$$

and the noise variance of $y_{p,i}$ is

$$V_i=if_sTN_0. \quad (51)$$

Since detection variables of the 1st and 2nd stages have non-central χ^2 distribution with DOF 2 for the H_1 cell and central χ^2 distribution with DOF 2 for an H_0 cell, the distribution of $y_{p,1}$ and $y_{p,2}$ for the H_1 cell can be found as

$$P_{al}(y_{p,i})=\frac{1}{V_i}\exp\left[\frac{-\left(y_{p,i}+S_i^2\right)}{V_i}\right]I_0\left(\frac{2S_i\sqrt{Y_i}}{V_i}\right), \quad (52)$$

where i=1,2, $I_0(\cdot)$, is the zeroth-order modified Bessel function of the first kind, $y_{p,1}$ and $y_{p,2}$ the distribution of and for an H_0 cell is

$$P_{a0}(y_{p,i})=\frac{1}{V_i}\exp\left(\frac{-y_{p,i}}{V_i}\right), \quad (53)$$

where i=1,2. Using P_{a1} (Eq. (52)) and P_{a0} (Eq. (53)), we can find the false alarm, detection, and misdetection probabilities when four asynchronous correlators are used for a serial search scheme as shown in Fig. 3. The false alarm probability when the four hypotheses being tested are cells, detection probability, false alarm probability when one of the four hypotheses being tested are the H_1 cell, and misdetection probability are derived as (Kim & Kong 2014)

$$P_{F,i}(\gamma_i)=P_{a0}\left(y_{p,i}^{(N)}>\gamma_i\right)=1-\left[1-\exp\left(\frac{-\gamma_i}{V_i}\right)\right]^N \quad (54)$$

$$P_{D,i}(\gamma_i)=P_{a1}\left(y_{p,i}>\gamma_i\right)=Q_0\left(S\sqrt{\frac{2}{V_i}},\sqrt{\frac{2\gamma_i}{V_i}}\right) \quad (55)$$

$$\begin{aligned}P_{f,i}(\gamma_i)&=P_{a0}\left(y_{p,i}^{(N-1)}>\gamma_i\right)\cdot P_{al}\left(y_{p,i}<\gamma_i\right)\\&=\left[1-\left(1-\exp\left(\frac{-\gamma_i}{V_i}\right)\right)^{N-1}\right]\times\left[1-Q_0\left(S_i\sqrt{\frac{2}{V_i}},\sqrt{\frac{2\gamma_i}{V_i}}\right)\right]\end{aligned} \quad (56)$$

$$P_{M,i}(\gamma_i)=1-P_{D,i}(\gamma_i)-P_{f,i}(\gamma_i), \quad (57)$$

where N (= 4) is the number of hypotheses being tested asynchronously, and $X^{(N)}$ denotes the N-th minimum of X.

5.3 Third Stage of the Proposed Technique

In the 3rd stage of the proposed technique, the detection variable has the same distribution to that of the DSB technique, so that the ACF peak for the H_1 cell is

$$S_3=\sqrt{y_{p,3}}, \quad (58)$$

and the noise variance is

$$V_3=4f_sTN_0. \quad (59)$$

For the H_1 cell, the distribution of $y_{p,3}$ is a noncentral χ^2 distribution with DOF 4 as

$$P_{b1}(y_{p,3})=\frac{1}{V_3}\exp\left[\frac{-(y_{p,3}+S_3^2)}{V_3}\right]\sqrt{\frac{y_{p,3}}{S_3^2}}I_1\left(\frac{2S_3\sqrt{y_{p,3}}}{V_3}\right), \quad (60)$$

and the distribution of $y_{p,3}$ for an H_0 cell has a central χ^2 distribution with DOF 4 as

$$P_{b0}(y_{p,3})=\frac{y_{p,3}}{V_3^2}\exp\left(\frac{-y_{p,3}}{V_3}\right). \quad (61)$$

Using P_{b1} (Eq. (60)) and P_{b0} (Eq. (61)), the false alarm probability when the four hypotheses being tested are H_0 cells, detection probability, false alarm probability when

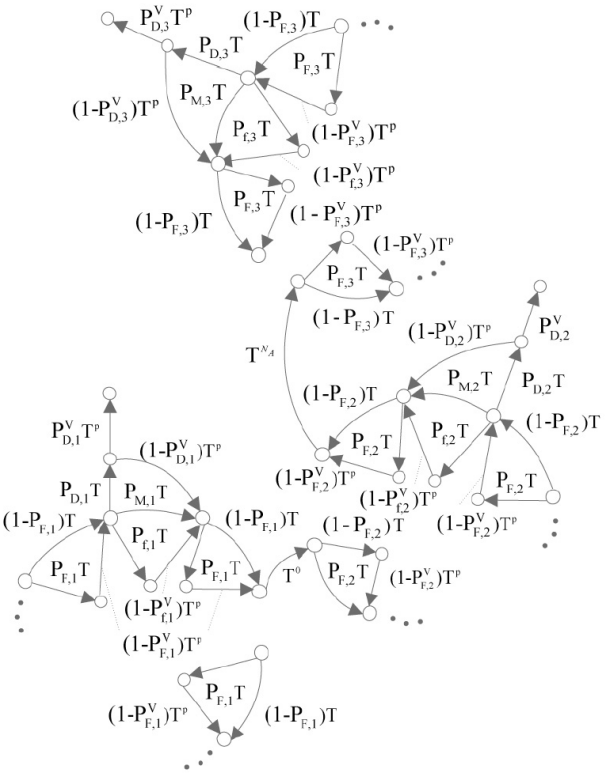

Fig. 5. Search state diagram.

one of the four hypotheses being tested are the H_1 cell, and misdetection probability are derived as (Kim & Kong 2014)

$$P_{F,3}(\gamma_3) = 1 - \left[P_{b0}\left(y_{p,3} < \gamma_3 \right) \right]^4 = 1 - \left[1 - \left[1 + \frac{\gamma_3}{V_3} \right] \exp\left(-\frac{\gamma_3}{V_3} \right) \right]^4 \tag{62}$$

$$P_{D,3}(\gamma_3) = P_{bl}(y_{p,3} > \gamma_3) = Q_2\left(S_3\sqrt{\frac{2}{V_3}}, \sqrt{\frac{2\gamma_3}{V_3}} \right) \tag{63}$$

$$P_{M,3}(\gamma_3) \approx P_{b1}\left(y_{p,3} < \gamma_3\right)\left[P_{b0}\left(y_{p,3} < \gamma_3\right)\right]^3 = \left[1 - Q_2\left(S_3\sqrt{\frac{2}{V_3}}, \sqrt{\frac{2\gamma_3}{V_3}} \right) \right] \times \left[1 - \left[1 + \frac{\gamma_3}{V_3} \right] \exp\left(-\frac{\gamma_3}{V_3} \right) \right]^3 \tag{64}$$

$$P_{f,3}(\gamma_3) = 1 - P_{D,3}(\gamma_3) - P_{M,3}(\gamma_3) \tag{65}$$

respectively.

5.4 Mean Acquisition Time

The search state diagram of the proposed technique is illustrated in Fig. 5. Each node represents four hypotheses that are simultaneously tested by the four asynchronous correlators. It shows that verification mode that takes pT seconds is initiated when a signal detection is declared at any stage, and that the technique moves to the $(i+1)$-th stage when signal is not detected by the end of the -th stage (i=1,2). Notice that the search state diagram shows a non-circular search scheme, where the search operation does not return to the 1st stage to re-initialize the search when signal is not detected by the end of the 3rd stage. Since when a GNSS receiver fails to detect a satellite signal, the receiver begins searching for another satellite signal rather than searching the satellite signal again.

Using Eqs. (54-57) and Eqs. (62-65), the mean acquisition time (MAT) of the proposed technique for a circular search scheme can be found as

$$\begin{aligned} H(T) = {} & \frac{1}{F_c(1 - H_{M,1}H_{0,1}^{F_c-1}H_{M,2}H_{0,2}^{F_c-1}H_{M,3}H_{0,3}^{F_c-1}N_AT)} \\ & \times \Bigg(H_{D,1}(T)\sum_{k=0}^{F_c-1} H_{0,1}^k(T) \\ & + H_{M,1}(T)H_{0,1}^{F_c-1}(T)H_{D,2}(T)\sum_{k=0}^{F_c-1} H_{0,2}^k(T) \\ & + H_{M,1}(T)H_{0,1}^{F_c-1}(T)H_{M,2}(T)H_{0,2}^{F_c-1}(T)H_{D,3}(T) \\ & \times N_AT\sum_{k=0}^{F_c-1} H_{0,3}^k(T) \Bigg), \end{aligned} \tag{66}$$

where F_c is the number of hypotheses in a stage, and $N_A = F_C$ indicates the time needed for the first half of the 3rd stage. The branch transfer functions for the correct hypothesis, the correct hypothesis missed, and an incorrect hypothesis are

$$H_{D,i}(T) = P_{D,i}T^{p+1} \tag{67}$$

$$H_{M,i}(T) = P_{M,i}T + P_{f,i}T^{p+1} \tag{68}$$

$$H_{0,i}(T) = (1 - P_{F,i})T + P_{F,i}T^{p+1}, \tag{69}$$

where i=1,2,3. On the other hand, for the non-circular search scheme as illustrated in Fig. 5, a practical search transfer function can be derived as

$$\begin{aligned} H_r(T) = {} & \frac{1}{F_c}\Bigg(H_{D,1}(T)\sum_{k=0}^{F_c-1} H_{0,1}^k(T) \\ & + H_{M,1(T)}H_{0,1}^{F_c-1}(T)H_{D,2}(T)\sum_{k=0}^{F_c-1} H_{0,2}^k(T) \\ & + H_{M,1}(T)H_{0,1}^{F_c-1}(T)H_{M,2}(T)H_{0,2}^{F_c-1}(T)H_{D,3}(T) \\ & \times N_AT\sum_{k=0}^{F_c-1} H_{0,3}^k(T) \Bigg) + H_{M,1}(T)H_{0,1}^{F_c-1}(T) \\ & \times H_{M,2}(T)H_{0,2}^{F_c-1}(T)H_{M,3}(T)H_{0,3}^{F_c-1}(T). \end{aligned} \tag{70}$$

Utilizing the algebraic method to obtain MAT introduced in (Viterbi 1995), the MAT of the proposed technique can be derived as

$$\mu = \left.\frac{dH_r(T)}{dT}\right|_{T=1}$$
$$\approx (p+1)P_{D,1} + (pP_{F,1}+1)P_{D,1}\frac{F_c-1}{2}$$
$$+ (P_{M,1}+P_{f,1})\left[(p+1)P_{D,2} + (pP_{F,1}+1)P_{D,2}\left(F_c - \frac{1}{2}\right)\right]$$
$$+ (P_{M,1} + (p+1)P_{f,1})(P_{D,2} + (P_{M,2}+P_{f,2})P_{D,3})$$
$$+ (P_{M,1}+P_{f,1})[P_{M,2} + (p+1)P_{f,2}P_{D,3}$$
$$+ P_{D,2}(pP_{F,1}+1)F_c + (P_{M,2}+P_{f,2})[F_c P_{D,3}(pP_{F,1}+1)$$
$$+ P_{D,3}(p+1+N_A) + F_c P_{D,3}(pP_{F,2}+1)$$
$$+ \frac{F_c-1}{2}P_{D,3}(pP_{F,3}+1) + (P_{M,3}+P_{f,3})(3(F_C+1)$$
$$+ pF_c(P_{F,1}+P_{F,2}+P_{F,3}) \quad (71)$$

For a comparison, the overall transfer function of the conventional SSB and DSB techniques can be expressed as

$$H_c(T) = \frac{1}{F_a}\left[H_D(T)\sum_{k=0}^{F_a-1}H_0^k(T)\right] + H_M(T)H_0^{F_a-1}, \quad (72)$$

where $F_a(=4F_c)$ is the number of total hypotheses to test, and

$$H_{D,i}(T) = P_{D,i}T^{p+1} \quad (73)$$
$$H_{M,i}(T) = P_{M,i}T \quad (74)$$
$$H_{0,i}(T) = (1-P_{F,i})T + P_{F,i}T^{p+1}, \quad (75)$$

where i=1,2,3. Using Eqs. (72-75), the MAT of the conventional SSB and DSB techniques can be expressed as

$$\mu_C = \left.\frac{dH_c(T)}{dT}\right|_{T=1}$$
$$= \frac{1}{F_a}[(p+1)P_D F_a + \frac{F_a(F_a-1)}{2}P_D(1+pP_F)]$$
$$+ P_M[1+(F_a-1)(1+pP_F)]. \quad (76)$$

6. NUMERICAL RESULTS

In this section, the performance of the proposed technique is demonstrated using 10^4 Monte Carlo simulations for a Galileo E5 receiver with two BPFs having $2f_r$ BW for E5a and E5b signals. Both E5a and E5b signals are sampled at the same sampling frequency $f_s = 2f_r$ and integrated with an interval T_0=1 ms to produce a search result. The total number of Doppler frequency hypotheses to test is $F_a = 20$ by choosing the Doppler frequency search step size of 525 Hz, which is a reasonable choice, since the Doppler frequency search step size can be from $1/(2T_0)$ to $2/(3T_0)$ (Kaplan & Hegarty 2005). And N_A= 5×20460 is the number of all hypotheses to search in the first half of the 3rd stage.

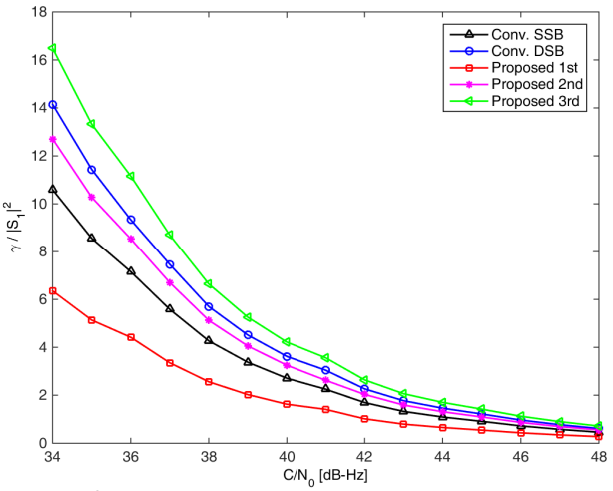

Fig. 6. γ with respect to C/N$_0$.

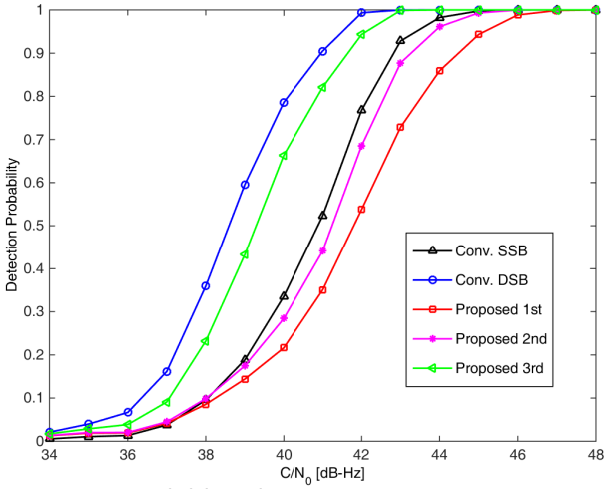

Fig. 7. Detection probability with respect to C/N$_0$.

Fig. 6 shows numerically evaluated detection threshold (for i=1,2,3) to the 1st stage signal power ratio, i.e., $\gamma_i/|S_1|^2$, to achieve a constant false alarm rate (CFAR) $P_F+P_f=10^{-3}$ in Eqs. (54, 56, 62, 65) for a wide range of the C/N_0 of the incoming Galileo E5a signal. Note that to achieve $P_F+P_f=10^{-3}$, it should be $\gamma_{i+1}>\gamma_i$ for i=1,2. Note also that γ_2 and γ_3 are larger than γ for the SSB technique and that for the DSB technique, respectively, which is because the proposed technique has a slightly higher false alarm probability, P_F+P_f, than the P_F (Eq. (46)) of the conventional SSB and DSB techniques for the same C/N_0 of the incoming signal.

Fig. 7 shows the detection probabilities P_D of the proposed technique and the conventional techniques for CFAR=10^{-3}. In general, the detection variable of the DSB technique is 3dB higher than that of the SSB technique. However, the detection threshold for the DSB technique is slightly higher than that for the SSB technique, which results in about 2 dB gain in the P_D. In addition, as expected from the comparison

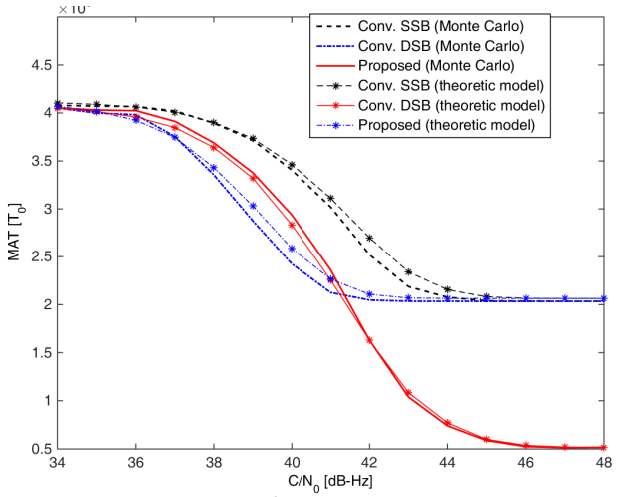

Fig. 8. Mean acquisition time with respect to C/N_0.

of the detection thresholds of the proposed technique to the conventional techniques in Fig. 6, the detection probabilities of the 2nd and 3rd stages of the proposed technique are slightly smaller than those of the SSB and DSB techniques, respectively. Note that the detection probability of the proposed technique increases as the stage increases, so that the proposed technique has multilevel detection sensitivity.

Fig. 8 shows the MAT from the 10^4 Monte Carlo simulations and from the numerical evaluation of the algebraic expressions in Eqs. (71, 76) for the non-circular search scheme. The theoretical MAT derived in subsection 5.4 matches the MAT's obtained from Monte Carlo simulations for the SSB, DSB, and proposed techniques. As expected, the proposed technique can achieve about 4 times faster acquisition for strong signals, and the MAT of the proposed technique is about the average of the SSB and DSB techniques for moderate and weak signals. Note that the MAT at low $C/N_0(\leq 36)$ dB shows a saturation, since the signal is not detectable and the MAT is mostly for testing all of the hypotheses in the two-dimensional hypothesis space once. Notice that the proposed technique shows a similar performance improvement to the multiple dwell search technique. However, the proposed technique is different from the multiple dwell search technique in that the proposed technique performs an asynchronous search and combines search results for different DSSS signals to improve sensitivity level. In addition, the multiple dwell search technique can be integrated into the proposed technique, which can further reduce the MAT, especially, for strong signals at high $C/N_0(\leq 42)$ dB. Therefore, the proposed technique can be very useful to quickly search and acquire the line-of-sight signals in open sky environments. Increasing the integration interval can be applicable to the proposed technique and the conventional SSB and DSB techniques with an appropriate change of the number of Doppler frequency hypothesis, and, in such a case, the MAT performances of the proposed technique and the conventional techniques show the same pattern with a positive C/N_0 gain to those plots in Fig. 8.

6. CONCLUSION

A fast AltBOC signal acquisition technique using an asynchronous search strategy has been proposed. The proposed technique can have multilevel detection sensitivity, which allowing a fast detection of the target signal when the signal strength is high enough. A complete algebraic analysis to evaluate the performance of the proposed technique has been provided, and it has been demonstrated with numerous Monte Carlo simulations that the proposed technique can achieve a multiple times smaller MAT than the conventional Galileo E5 primary code acquisition techniques for strong incoming AltBOC signals. Therefore, it can be found that the proposed technique is very useful for receivers to acquire the primary code of the Galileo E5 signals quickly in open sky environments.

ACKNOWLEDGMENTS

This research (2013R1A2A2A01067863) was supported by Mid-career Researcher Program through NRF grant funded by the Korean government (MEST).

REFERENCES

Abu-Rgheff, M. A. 2007, Introduction to CDMA Wireless Communications (CA: Academic Press)

Galileo Project, Galileo OS SIS ICD [Internet], cited 2013 July 13, available from: http://ec.europa.eu/enterprise/policies/satnav/index en.htm

Kaplan, E. D. & Hegarty, C. J. 2005, Understanding GPS: Principles and Applications, 2nd ed (MA: Artech House)

Kim, B. & Kong, S.-H. 2014, Determination of detection parameters on TDCC performance, IEEE Trans. Wirel. Commun., 13, 2422-2431, http://ieeexplore.ieee.org/stamp/stamp.jsp?tp=&arnumber=6733255

Lestarquit, L., Artaud, G., & Issler, J. L. 2008, AltBOC for dummies or everything you always wanted to know about AltBOC, in ION ITM, Savannah, GA, Sep 2008

Marcum, J. I. 1950, A Table of Q-functions, Rand Corp.

Report, RM-339, Jan. 1950

Margaria, D., Dovis, F., & Mulassano, P. 2008, Galileo AltBOC signal multiresolution acquisition strategy, IEEE Trans. Aero. Electr. Sys., 23, 4-10, http://dx.doi.org/10.1109/MAES.2008.4693984

Misra, P. & Enge, P. 2006, Gobal Positioning System: Signals, Measurements, and Performance, 2nd ed (MA: Ganga-Jamuna Press)

Montenbruck, O., Hauschild, A., Steigenberger, P., Hugentobler, U., Teunissen, P., et al. 2012, Initial assessment of the COMPASS/BeiDou-2 regional navigation satellite system, GPS Sol., 17, 211-222, http://dx.doi.org/10.1007/s10291-012-0272-x

Parkinson, B. W., Spilker, Jr, J. J., Axelrad, P., & Enge, P. 1996, Gobal Positioning System: Theory and Applications (Washington, DC: AIAA, Inc.)

Shivaramaiah, N. C. 2011, Enhanced Receiver Techniques for Galileo E5 AltBOC Signal Processing, PhD Dissertation, School of Surveying and Spatial Information Systems, University of New South Wales, Sydney, Australia

Sleewaegen, J. M., Wilde, W. D., & Hollreiser, M. 2004, Galileo AltBOC receiver, in ENC GNSS, Rotterdam, The Netherlands, 17-19 May 2004

Viterbi, A. J. 1995, CDMA: Principles of Spread Spectrum Communication (CA: Addison-Wesley Publishing Company)

Wallner, S., Hein, G. W., Pany, T., Avila-Rodriguez, J. A., & Posfay, A. 2005, Interference computations between GPS and Galileo, in ION GNSS, Long Beach, CA, USA, 13-16 Sep. 2005

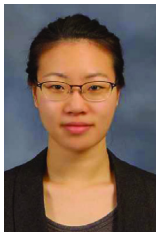

Binhee Kim received B.S. and M.S. degrees in electrical engineering from Korea Advanced Institute of Science and Technology (KAIST), Daejeon, Korea, in 2008 and 2010, respectively. She is a researcher in the CCS Graduate School for Green Transportation at KAIST, where she received a Ph.D. degree in 2015. Her research interests include radar signal processing, GNSS signal processing, and detection and estimation for navigation systems.

Seung-Hyun Kong received a B.S.E.E. from Sogang University, Korea, in 1992, an M.S.E.E. from Polytechnic University, New York, in 1994, and a Ph.D. degree in aeronautics and astronautics from Stanford University, CA, in 2006. From 1997 to 2004, he was with Samsung Electronics Inc. and Nexpilot Inc., both in Korea, where his research focus was on 2G CDMA and 3G UMTS PHY and mobile positioning technologies. In 2006, he was involved with hybrid positioning technology development using wireless location signature and Assisted GNSS at Polaris Wireless, Inc. and from 2007 to 2009, he was a research staff at Qualcomm Research Center, San Diego, CA, where his R&D focused on indoor location technologies and advanced GNSS technologies. Since 2010, he has been an Assistant Professor at the Department of Aerospace Engineering in the Korea Advanced Institute of Science and Technology (KAIST). His research interests include super-resolution signal processing, detection and estimation for navigation systems, and assisted GNSS in wireless communication systems.